JOURNAL OF SOLID STATE CHEMISTRY 48, 256–271 (1983)

Structure of Small Defects in Nonstoichiometric WO_{3-x}

L. A. BURSILL

School of Physics, University of Melbourne, Parkville, 3052, Victoria, Australia

Received December 6, 1982

Structural models are derived for the hitherto "unresolved" small defects which should occur in the nonstoichiometric phase WO_{3-x}. The mechanisms of aggregation or interaction of these small defects to produce extended defect structures (i.e., crystallographic shear planes and pentagonal and/or hexagonal tungsten bronze-type columns) are discussed next. Linear defects, consisting of two pairs of edge-shared octahedra, are proposed. These readily explain the large number of electron microscope observations of precipitation and dissolution phenomena reported for reduced WO_{3-x} and doped tungsten trioxide specimens.

1. Introduction

Considerable uncertainty remains concerning the nature of the structural defects responsible for the nonstoichiometric phase WO_{3-x} (*1*). A thermodynamic study using emf measurements revealed a single phase between WO_3 and $WO_{2.9760}$ for temperatures in the range 700–900°C (*1*). The results were interpreted in terms of point defect structures, namely singly-ionized oxygen vacancies $V_{\dot{0}}$, between WO_3 and $WO_{2.9880}$. However, the reason given for preferring $V_{\dot{0}}$, rather than the tungsten interstitial $W_i^{5\cdot}$ which was equally consistent with the law of mass action analysis, was simply stated as due to the difficulty of imagining isolated interstitial tungsten, randomly distributed without formation of arrays of crystallographic shear planes (*CSP*). For larger departures from stoichiometry the variations of $\Delta H(O_2)$ and $\Delta S(O_2)$ suggested the formation of more complex defects (*1*). Electrical conductivity measurements (*2*) revealed a dependence on partial pressure of oxygen of the form $\sigma \propto p_{O_2}^{-\frac{1}{4}}$, which was interpreted as indicating the presence of doubly-ionized oxygen vacancies $V_{\ddot{0}}$. Berak and Sienko (*3*) proposed a single phase WO_3–$WO_{2.9873}$ containing small crystallographic shear planes bounded by partial dislocation loops (*4*).

High-resolution electron microscopy (HREM) has revealed at least three types of extended defects in both slightly reduced WO_{3-x} and in doped WO_3 crystals. These include (i) crystallographic shear planes (*CSP*; Refs. (*5–8*), (ii) pentagonal bipyramidal columns (PC; Refs. (*7–10*), and (iii) hexagonal tunnels (HTB; Refs. (*10, 11*)). The nature of the extended defects observed is critically dependent upon the initial stoichiometry and temperature of formation, whether specimens are prepared in reduction or oxidation, and upon any subsequent cooling history. Often more than one type of extended defect structure is observed in the same specimen (see, e.g., Refs. (*10,*

0022-4596/83 $3.00

11)), and sometimes defects appear during observation in the electron microscope (*6*).

It is the purpose of this paper to develop structural models for hitherto "unresolved" small defects which should occur in the nonstoichiometric phase WO_{3-x}. The mechanisms of aggregation and interaction of such small defects to produce extended defect structures on crossing this phase boundary, either on cooling from high temperature, or by increasing the degree of reduction, are examined next.

2. Derivation of Interstitial Defect Structures

CSP in WO_{3-x} contain, as a common structural principle, zigzag edge-shared sets of octahedra linked by corner-sharing in such a way that they may be regarded as coherent intergrowths of elements of the *R*-Nb_2O_5-type structure within the WO_3 matrix (*5*). The HREM observation (*8*) that pairs of closely spaced *CSP* occurred frequently in specimens of Ta-doped WO_3, quenched from temperatures which presumably lie within the WO_{3-x} phase, suggests that the small defects existing at high temperatures may contain structural elements which also exist within a pair of *CSP*. (The argument used here closely follows that used in Ref. (*12*) for the derivation of small linear defect models in TiO_{2-x} ($0 \leq x \leq 0.0035$). These models successfully account for a wide range of *CSP* and platelet precipitation and dissolution phenomena recently studied by HREM in reduced and doped rutiles (*13–18*). Such small defects should be readily mobile and able to aggregate to allow *CSP* and/or PC and/or HTB extended defects to precipitate on cooling across the WO_{3-x} phase boundary or on reduction in an electron beam. Similarly the extended defects should be able to readily dissolve on heating or oxidation, see, e.g., Ref. (*19*). It is convenient to begin with the precipitation of pairs of *CSP* and then extend the discussion to other extended defects.

(*a*) *Small Defects and Precipitation of Pairs of CSP*

Figures 1a–d show the octahedral arrangement for a [010] projection through pairs of (102), (103), (104), and (001) *CSP*, respectively. Note that cations in edge-shared octahedral sites (heavily lined in Fig. 1) must have, formally at least, charge +5 if the correct stoichiometry (W^{6+}_{n-1}, M^{5+}) O_{3n-p} is to be achieved (see Ref. (*5*)

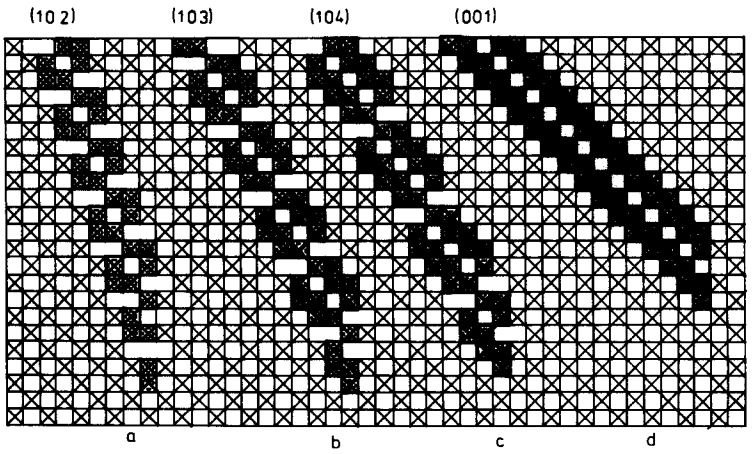

FIGS. 1a–d. Octahedral arrangements for [010] projections through pairs of (102), (103), (104), and (001) *CSP* in WO_3 matrix. M^{5+} cation sites (heavily lined) edge-shared octahedral sites.

for definition of **n** and **p**). The degree of localization of electronic charge on these sites is still an unresolved problem (*3*).

Inspection of Figs. 1a,b,d shows that in each case there is only one way to decompose the *CSP* pairs into *identical* units which are commensurate with an essentially undeformed WO_3 matrix. These are shown heavily lined in Figs. 2a–c. Note that we have in fact derived a series of [101] linear defect structures containing pairs of edge-shared octahedra at either end which are separated by strips of alternately filled and empty octahedral sites along the length of the defect. These three linear defects may be readily interconverted by the atomic displacements indicated by arrows in Figs. 2a–c. Note (i) that aggregation of such defects leads naturally to formation of *CSP* pairs, without the necessity of creating a partial dislocation loop (cf. Figs. 1, 2), (ii) to complete the octahedral coordination of the displaced W atoms it is necessary to place additional oxygen atoms into the originally empty sites at the centers of the cubo-octahedral interstices of the framework, at both top and bottom of the inserted and displaced W atoms. This feature of the defect model is illustrated in Fig. 3a for the smallest defect, and is crucial in modeling small defects, since these must be bounded or surrounded completely by essentially unchanged WO_3 host crystal. Thus the drawings of Figs. 2a–c represent sections, or bounded projections, and *not* projections as is the case for Fig. 1. Inspection of Fig. 3a shows that to create an almost neutral defect, which will minimize electrostatic energy, it is necessary to make it two octahedra high, thus amounting to adding W_2O_5 and in addition, replacing $6W^{6+}$ cations by six W^{5+} cations, as shown in Figs. 2a and 3a. This smallest defect is of the type required to produce (001) *CSP* pairs by aggregation and alignment (Fig. 1d). The corresponding $[10\bar{1}]$ sections through the extended defects required to directly form pairs of (103) and (102) *CSP* are shown in Figs. 3c,d. Extension of the defect along [101] requires insertion of an extra O_2 unit for each stage. Thus (102)-type small defects are most oxygen rich, but still reduced overall from WO_3, followed by (103), then (001). This sequence is in fact observed for

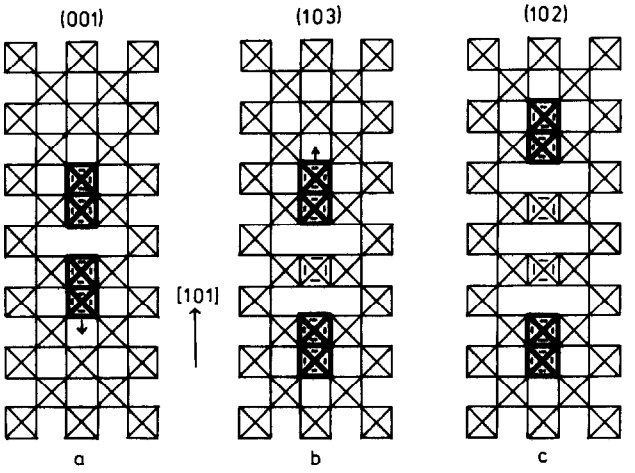

FIGS. 2a–c. Linear defects parallel to [101] (heavily lined) required for precipitation of pairs of (001), (103), and (102) *CSP*. Note defects contain pairs of edge-shared octahedra at each end, with a string of displaced octahedra linking these. The three distinct linear defect models are readily interconverted by atomic displacements indicated by arrows.

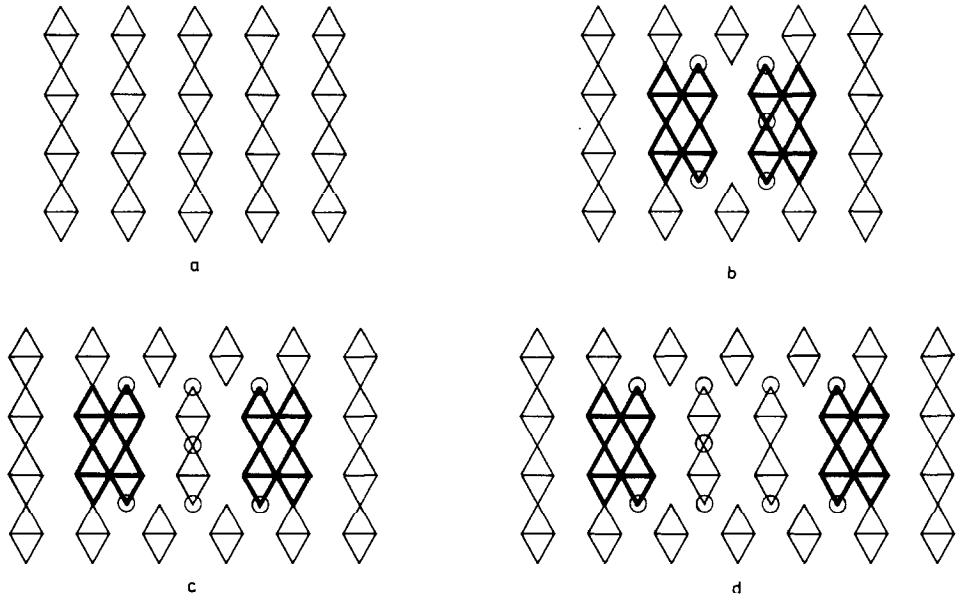

FIGS. 3a,b. [10$\bar{1}$] projection showing addition of W_2O_5 units, including oxygens at top and bottom of WO strings for displaced and inserted octahedra, required to produce (001) type small defects.

FIGS. 3c,d. Additional O_2 pairs added to terminate (103)- and (102)-type linear defects. Circles indicate added oxygen.

(10*l*) *CSP* for increasing degrees of reduction (see, e.g., Ref. (*20*), Table V). This would imply that the extension of the linear defects (i.e., their length) depends upon x in WO_{3-x} and/or upon temperature. Thus the distribution of *CSP* orientations observed in any specimen will depend critically upon x and the rate of cooling across the WO_{3-x} phase boundary. A statistical distribution of linear defects having several lengths at high temperatures will be reflected as variations in orientation, with local disorder along individual *CSP* after precipitation at lower temperatures. In fact (104) *CSP* require an ordered mixture of (103)- and (001)-type linear defects in the ratio 2 : 1 (Fig. 1c).

Note that there are eight W^{5+} cations involved in each linear defect (Figs. 3a,b,c). In the shortest defect six of these have replaced $6W^{6+}$ cations and an additional W_2O_5 has been incorporated "interstitially." This implies of course that oxygens (*3*) have also been lost from the surface to the gas phase. For each successive extension of the linear defect it is necessary to incorporate a further two oxygens "interstitially" to complete octahedral coordination for displaced W^{6+} cations (Figs. 3c,d). Thus larger defects are effectively less reduced. (The maximum extension possible would correspond to adding a total of 14 oxygens giving length 9 × [101] (≃ 50 Å) and would correspond to *CSP* orientation very close to (101). So far there is no evidence that extension greater than that corresponding to (102) *CSP* (i.e., ≃ 25 Å, Fig. 3d) occurs in WO_{3-x}. This confirms that it is relatively easier to remove oxygen from the surface than to incorporate additional oxygens internally.)

Figure 4 indicates atomic jumps which enable mobility of the "interstitial" defect, as required for precipitation of pairs of *CSP*. It is assumed that on reduction these small defects are created at the crystal surfaces and subsequently diffuse into the bulk

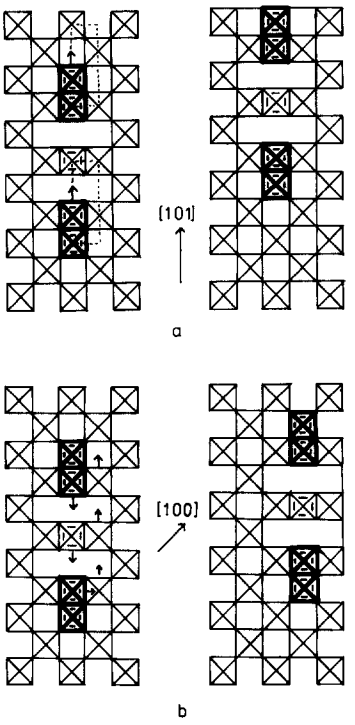

FIG. 4. Atomic displacements (arrowed) required for mobility of (103)-type linear defects parallel to [101] (a) and parallel to [100] (b). Dotted arrows (a) give corresponding cooperative diffusive steps required for M^{5+} cations (M = Nb, Ta).

crystal to produce a homogeneous distribution. This requires long-range diffusion of oxygen but presumably W^{5+} cations may be transported effectively, or at least partially, by a counter flow of electrons generated by the ionization reaction $W^{5+} \rightarrow W^{6+} + e^-$. In the ternary systems Nb–W–O and Ta–W–O long-range diffusion of both M^{5+} cations and oxygens are required and a more complex, but still straightforward, cooperative diffusion mechanism may be invoked (dotted in Fig. 4a). It has been assumed so far that W^{5+} ions remain in the edge-shared octahedral sites. This will presumably be the case only for relatively low temperatures. However, the emf, electrical conductivity, or other physical property measurements (1–3) have not, as yet, determined with any degree of certainty the nature of the conducting species, or the extent of any delocalization of electrons. The discussion given in pp. 126–132 of Ref. (*3*) is especially interesting.

To produce a *CSP* pair extending parallel to the projection axis of Figs. 1 and 2 it is necessary to transfer some oxygen ions out of their positions in the tunnels (Fig. 3) so that the small defects can coalesce, giving eventually infinite . . . O–W–O–W . . .

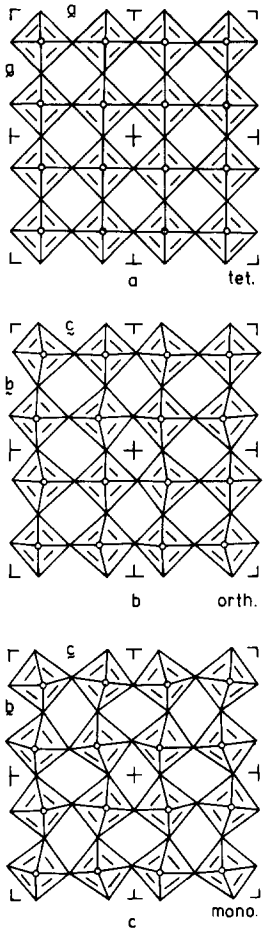

FIG. 5. Comparison of octahedral distortions and tilts for the tetragonal high temperature (>740°C) (a) orthorhombic (<710°C) (b) and monoclinic (c) phases of WO_3. The former is more coherent with the edge-shared strips of octahedra found in *CSP* structures (cf. Fig. 1), whereas the latter (b,c) are more coherent with the PC–HT, TTB, and HTB/ITB type defect structures.

chains extending along [010]. Such oxygens may be transported via cubo-octahedrally coordinated interstitial sites (e.g., those normally occupied by Ba in $BaTiO_3$). Alternatively some of these oxygens may stay in the tunnels leading to fractional occupancies and local disorder within the *CSP* structure.

Note that the octahedra in WO_3 do not have the ideal ReO_3-type structure used in Figs. 1–4 so far. A series of phase transitions have been reported for WO_3 (*21*). Thus an orthorhombic/tetragonal transformation occurs, with some hysteresis, in the temperature range 710–740°C. A further transformation from orthorhombic to monoclinic takes place at 330°C (*22*). Figures 5a–c compare octahedral tilts and deformations for these three structures. Thus the higher temperature (>740°C) tetragonal phase has a Slater-type mode of deformation (parallel to the projection axis in Fig. 5a) without octahedral tilts, whereas the orthorhombic phase (<710°C) has an additional torsional mode giving small octahedral tilts, in addition to distortions within octahedra (Fig. 5b). In the room temperature (<330°C) monoclinic phase another torsional mode in the *ab* plane becomes soft with tilt axes along **c**. This gives rise to an octahedral tilt structure exhibiting (approximately) a 4.3.4.3 net (Fig. 5c). It is interesting that the TTB (tetragonal tungsten bronze) and HTB structure types also approximate to this type of net (see drawings below and Refs. (*10, 11*)), whereas the *CSP* phases, with their strips of zigzag edge-shared octahedra, tend to impose a more regular arrangement of octahedra. Thus we expect that *CSP* will precipitate more readily at relatively high temperatures.

(*b*) *Small Defects Required for Precipitation of PT/HTB Structure Elements*

Sahle and Sundberg (*10*) observed PC/HTB elements in HREM studies, having various arrangements of PT–HC defects in {102} and {103} *CS* phases. These units also occur as defective regions within the HTB and intergrowth tungsten bronze (ITB)-type phases (*11*). The PC–HT structure was also seen to form during observation in the electron microscope, together with new *CSP*. Whenever a single *CSP* terminates within a WO_3 matrix it often does so at a defect consisting of PC–HT units (*10, 11*). This PC–HT structural unit is found also within the phases Mo_5O_{14}, $W_{18}O_{49}$ and a 2 : 5 preparation in the WO_3–Nb_2O_5 system (*10*). Both Refs. (*10*, Fig. 3a) and (*23*, Fig. 8) show black spot contrast which appears premonitory to growth of *CSP* during observation of WO_{3-x} crystals in the electron microscope. A comparison of oxygen elimination for different structure types shows that the reduction per unit distance increases in the order {102} *CSP*, {103} *CSP*, and {101} PC–HT planes.

The PC–HT structural element is shown

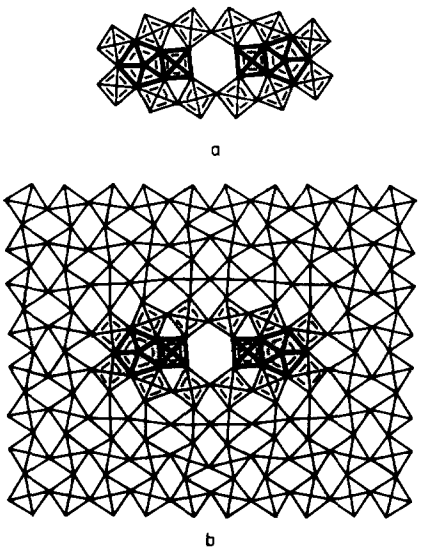

FIG. 6a. PC–HT structural unit derived by Sahle and Sundberg (*10*).

FIG. 6b. Insertion of PC–HT unit within WO_3 matrix. Note formation of small extrinsic platelet-shaped defect having expansion vector approx. 0.7**a** normal to cube planes.

in Fig. 6a. This structure may be inserted within a WO_3 matrix as shown in Fig. 6b. Note, however, that whereas it is readily compatible with the tilted octahedral framework (orthorhombic or room temperature monoclinic (*22*) forms of WO_3) it would introduce a high degree of long-range elastic or torsional strain into the high-temperature tetragonal WO_3 phase. It would therefore appear that the PC–HT units may be preferred in lower temperature preparations, or in specimens which were initially within the WO_{3-x} phase boundary, and then cooled rapidly (i.e., within the monoclinic or orthorhombic WO_3 regions) before precipitation of small defects could occur.

To create a small defect related to the PC–HT structural unit, which in Fig. 6b has infinite extent along the projection axis, it is necessary to envelope part of this unit entirely by WO_3. This may be readily achieved as shown in Fig. 7, where the inserted unit has stoichiometry $W_8O_{20} = 4W_2O_5$. Again the "interstitial" defect is two octahedra high along the projection axis (Fig. 7a). Termination within an envelope of WO_3 requires oxygens at top and bottom as shown in Figs. 7a,b. This defect has some of the characteristics of a very small interstitial loop or precipitate. The incorporation of additional tungsten and oxygen ions necessitates a dilation of the lattice, whereas the first "interstitial" defect, introduced above, was coherent with the lattice. Hereafter we refer to this first defect as the *CSP*-pair or *CSP*-P defect.

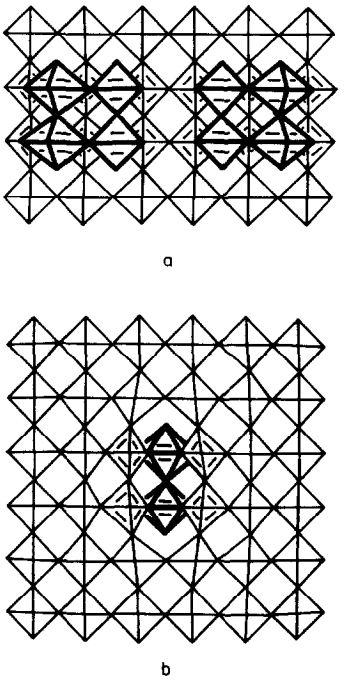

FIG. 7. PC–HT defect enveloped within WO_3 matrix by addition of oxygens at top and bottom of W–O strings to give overall stoichiometry $4W_2O_5$ (a) and give [100] and [001] projections (b).

(*c*) *Transformation of CSP-P into PC–HT Defects*

Each PC–HT unit contains $4W_2O_5$ in "interstitial" sites, whereas a *CSP*-pair defect contains interstitial W_2O_5. Thus four *CSP*-P defects should be consumed to precipitate one PC–HT unit. Each *CSP*-P defect also has associated with it $6W^{5+}$ cations which would imply occupancy of all PC–HT sites involving octahedra sharing edges with pentagonal bipyramidal polyhedra by W^{5+} cations. It is remarkable that there are just 24 of these. A detailed atomic mechanism for coalescence of four *CSP*-pair defects to form one PC–HT unit is difficult to draw but Figs. 8a,b show rectangular-shaped blocks of WO_{3-x} structure possessing topologically equivalent borders 8 × 4 octahedra in extent. In Fig. 8b two *CSP*-P units are drawn within this border and location of octahedra indicated with respect to the positions adopted in the corresponding PC–HT unit (Fig. 8c). A further two *CSP*-P units are added in Fig. 8b; note the location of additional W^{5+} ions, as indicated by shading. Clearly the detailed atomic movements are complex to describe but the process is straightforward in principle. (A possible intermediate stage is depicted in Fig. 16 below.) It is important to note that (i) in

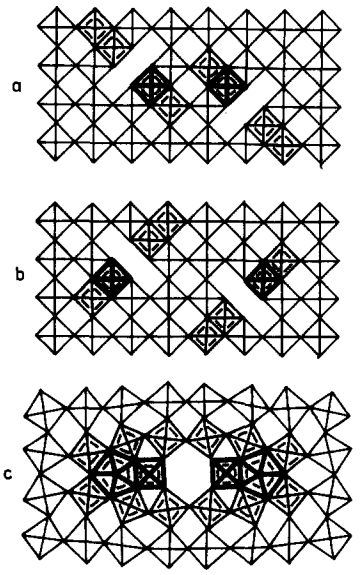

FIG. 8. Rectangular blocks of WO_3 containing topologically equivalent borders 8 × 4 octahedra in length. Two *CSP*-pair defects are drawn in (a) and (b) to indicate location of "interstitial" W^{5+} cations after precipitation of four *CSP*-pair defects to form one PC–HT unit (c).

Fig. 8 the second pair of *CSP*-P units are oriented orthogonal to the first; (ii) the precipitation of *CSP*-P units as PC–HT defects will certainly be enhanced by cooling from higher temperatures and involve the onset of octahedral tilts or torsional modes at the tetragonal/orthorhombic or orthorhombic/monoclinic phase transitions; (iii) an additional elastic strain (of relatively long range) will accompany the precipitation of PC–HT units, since these are much less coherent with the WO_3 matrix; (iv) the PC–HT precipitates have lenticular shape lying on {100} planes and have extrinsic displacement vector of magnitude approximately one octahedral edge (2.7 Å or $0.71a$). Growth of columns of PC–HT structure may occur by aggregation of either the *CSP*-P or PC–HT defects proposed above. Consideration of atomic diffusion mechanisms suggests that the *CSP*-P defect is more readily mobile and thus it may be that PC–HT columns in fact grow by aggregation of the *CSP*-pair units. This would have the additional attraction of facilitating the transport of the excess oxygens which need to be eliminated or dispersed as finite strings of stoichiometry O–W–O–W–O in the small defect are replaced by extended –O–W–O–W– strings in the columnar structure. Disorder, in the form of partially occupied pentagonal tunnel sites, is readily accommodated by this mechanism.

3. Discussion

(*a*) *Relationship of CSP-Pair Defects to Tetragonal Tungsten Bronze (TTB) Columnar Defects*

Figures 9a,b show how *CSP*-pair defects may readily transform into a TTB defect. In this case two *CSP*-P units are required to contribute $2W_2O_5$ each, with the additional W^{5+} ions distributed as indicated in the figure. It is envisaged that TTB columnar defects grow by aggregation of further *CSP*-P defects, since the corresponding two-octahedra high defects would appear to have

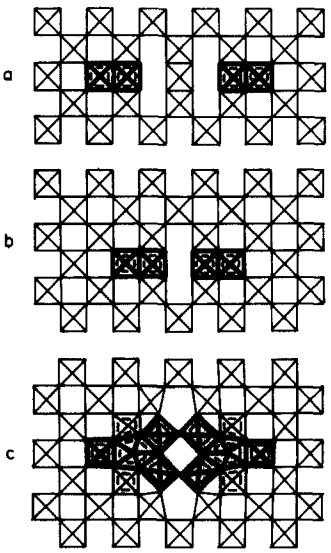

FIG. 9. Transformation of two *CSP*-pair-type defects (a,b) into one TTB-column defect (c).

relatively low mobility (see also Fig. 15 below). Isolated TTB columnar defects have been observed in Nb_2O_5–WO_3 preparations (*24*). Earlier (*25, 26*) a rotation screw disclination mechanism was used to relate the TTB-structure types to WO_3. However, it is now clear that TTB columns are more realistically generated by precipitation of the *CSP*-pair defects described here, obviating the necessity for concerted rotation of a square column of four corner-shared octahedra.

(*b*) *Formation of HTB Lamellae within* WO_3

HTB arrays may be formed within WO_3 matrix by construction of regular zigzag arrays of PC–HT units during precipitation (see structural drawings Fig. 2b in Ref. (*10*), and Figs. 4a,b in Ref. (*11*)).

Alternatively the PC–HT unit precipitated may itself be extended along [100] as indicated in Fig. 10, when linear precipitates of HTB structure occur, terminated by pentagonal bipyramidal units. Thus for each successive hexagonal tunnel included additional *CSP*-pair defects are required. Again it is envisaged that HTB lamellae are relatively immobile and grow along the projection axis by the aggregation of further *CSP*-pair defects.

Lamellar growth of such platelet shaped precipitates readily explains also the geometry of the HTB and ITB polytypic forms reported in Ref. (*11*).

(*c*) *Alternative "Vacancy" Mechanisms for* CSP *and PC Precipitation*

It has long been argued that *CSP* may grow by the aggregation of oxygen vacancies into discs on (102), (103), . . ., etc. planes (*27*) which then collapse by a partial dislocation mechanism (*4*) or by growth involving a hairpin topology and diffusion of altervalent cations from the surface, *without* the necessity to form *either* point defects or a partial dislocation (*28, 29*).

It is significant that the terminations of *CSP* observed in WO_{3-x} are *not* classical partial dislocations (Refs. (*10, 11*) and Fig. 11a), but involve PC–HT units as illustrated in Fig. 11b. (Note that this drawing shows the termination completely enveloped by WO_3, with some small but significant alterations to the model proposed in Ref. (*10*), Fig. 3b.) Furthermore inspection of the lattice images and structural drawings for a number of terminating single *CSP* shows that there is an expansion of the lattice around the termination—*not* a collapse—as required for an "interstitial" rather than vacancy-type small defect.

In Ref. (*10*) the authors proposed that PC units may be formed by removal of oxygens and consequent rearrangements as shown in their Fig. 10. However, no mechanisms were given (e.g., in the form of a structural drawing) whereby (i) such an operation could occur enveloped by WO_3, (ii) such a columnar unit (PC) could be formed by ag-

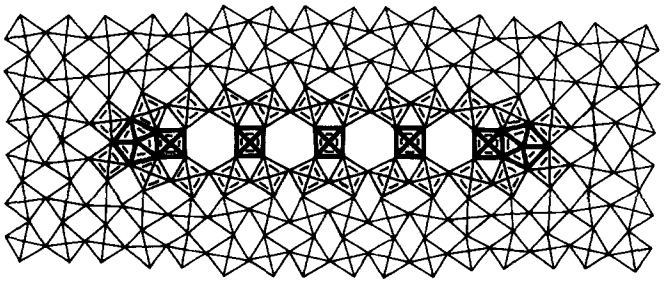

FIG. 10. HTB platelet within WO_3 matrix by extension of PC–HT defect. Note termination of HTB slab by pentagonal bipyramidal columns (cf. Figs. 6, 8).

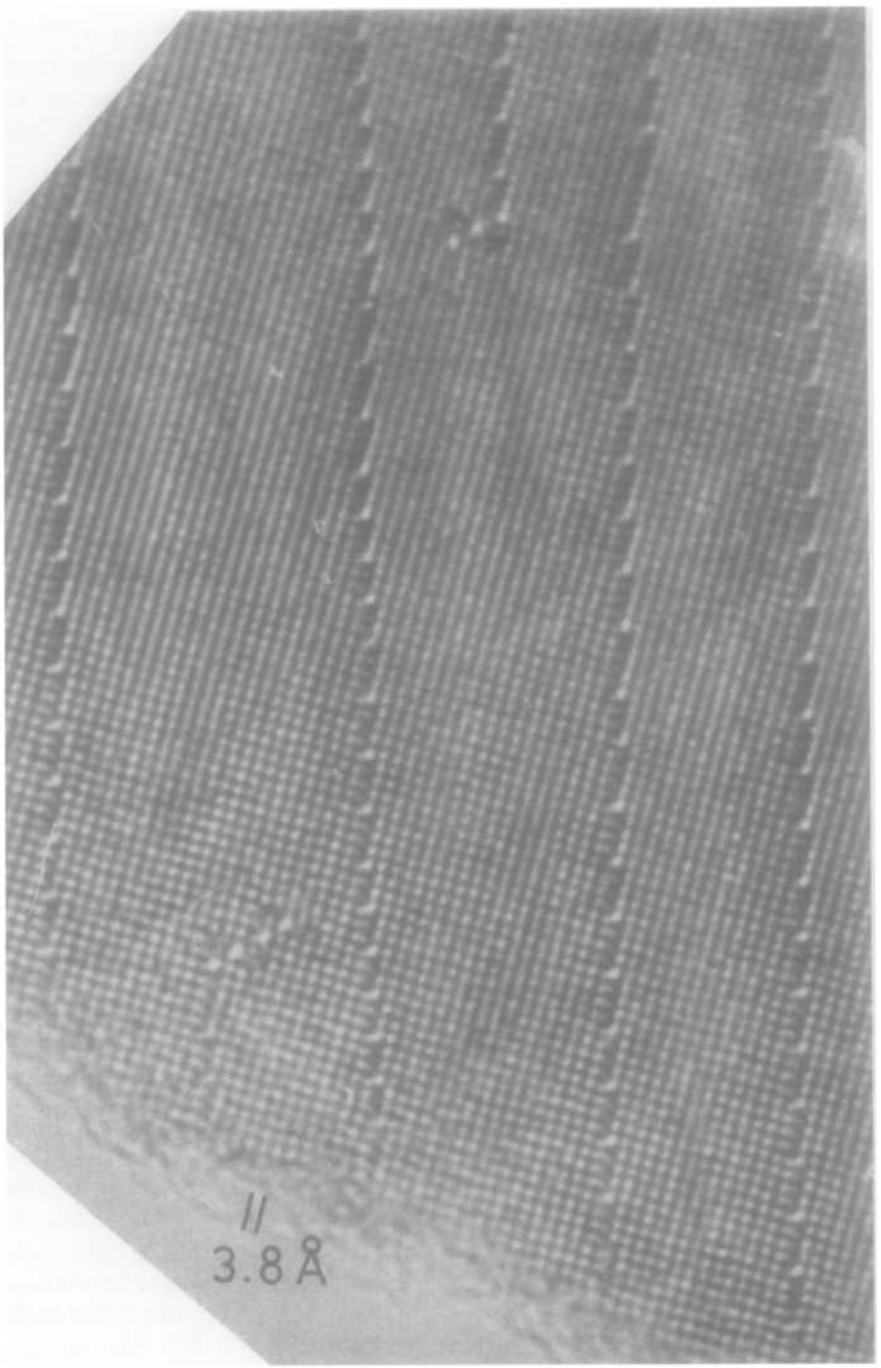

FIG. 11a. HREM image of $(Nb,W)O_{2.933}$ (powders reacted at 1350°C, heated for 5 days at 1350°C, then cooled to room temperature over several minutes) showing termination of single (104) *CSP* within a lamellae of existing *CSP*.

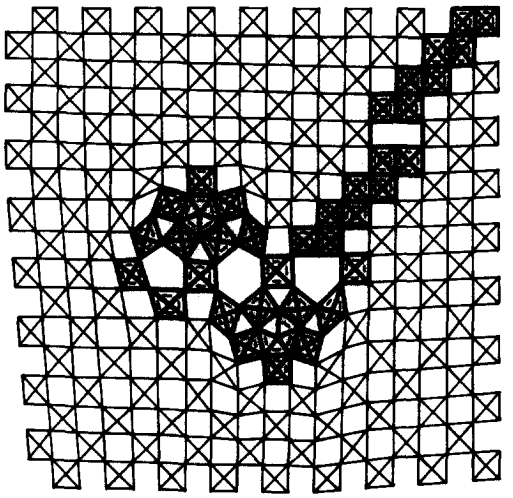

FIG. 11b. Structural model for termination of (104) *CSP* involving PC–HT unit. Note extrinsic nature of termination indicating interstitial, rather than vacancy, nature for *CSP* and for the PC–HT unit.

gregation of smaller, hitherto unresolved, defects, or (iii) these PC units could combine to form the PC–HT unit. It seems to the present author that the important result of Ref. (*10*) is the recognition of the PC–HT unit as a structure-building element. The above interstitial defects and mechanisms then readily explain the phenomena of precipitation of PC–HT units without invoking oxygen vacancies. Furthermore the phenomena of PC–HT structures occurring in the doped systems WO_3–Nb_2O_5 and WO_3–Ta_2O_5 or WO_3–TiO_2 are encompassed by the "interstitial" mechanisms described above, whereas the vacancy mechanisms have not addressed this subject.

(*d*) *Growth of Single* CSP *by Aggregation of Small Defects*

It may be seen from Figs. 1 and 2 that aggregation of *CSP*-pair defects readily explains the observation of *CSP*-pair precipitation in Ta_2O_5-doped WO_3 quenched from near melting point temperatures (*8*). It is more difficult to see how *single CSP* may form *directly* from such small defects. Inspection of the terminations of single *CSP* (see, e.g., Fig. 11a,b above) shows them to contain PC–HT units. Furthermore the images and structural drawings of such terminations show them to have an "interstitial" or extrinsic nature (Ref. (*10*), Fig. 10a,b; present Fig. 11a,b). These observations suggested that single *CSP* form at relatively low or intermediate temperatures where *CSP*-P defects are relatively unstable with respect to precipitation of PC–HT defects. Again a single *CSP* would be somewhat more coherent with a 4.3.4.3-type octahedral net than is a pair of *CSP*. Beam heating observations showed growth of single *CSP* [*23, 6, 7*] at presumably relatively low temperatures. The published images in these cases appear *not* to show PC–HT unit-type terminations. We therefore considered the possibility that PC–HT terminations may in fact represent precipitation of excess *CSP*-P units at lower temperatures, after single *CSP* have formed.

Figures 12a,b show two single *CSP* terminations, forming a sequence with Fig. 11b. There are two pentagonal columns (only one of which is filled) in Fig. 12a. The smallest termination contains only one empty pentagonal column (Fig. 12b). Figure 12c shows a short element of (103) *CSP* terminated at both ends. These drawings thus provide a detailed atomic model for the partial dislocations which accompany precipitation of *CSP* by an "interstitial" mechanism. An attractive feature of this model is that the termination is simply an empty pentagonal column (Fig. 12b) which may readily transform into filled pentagonal and empty hexagonal columns (Fig. 12a) and PC–HT units. Thus elastic (and electrostatic) deformation of the WO_{3-x} matrix is minimized, since the "dislocation" stereochemistry satisfies reasonable electrostatic and chemical bonding requirements, unlike the "cut-and-stick" models of classical dislocation theory.

The mechanism by which small *CSP*-P

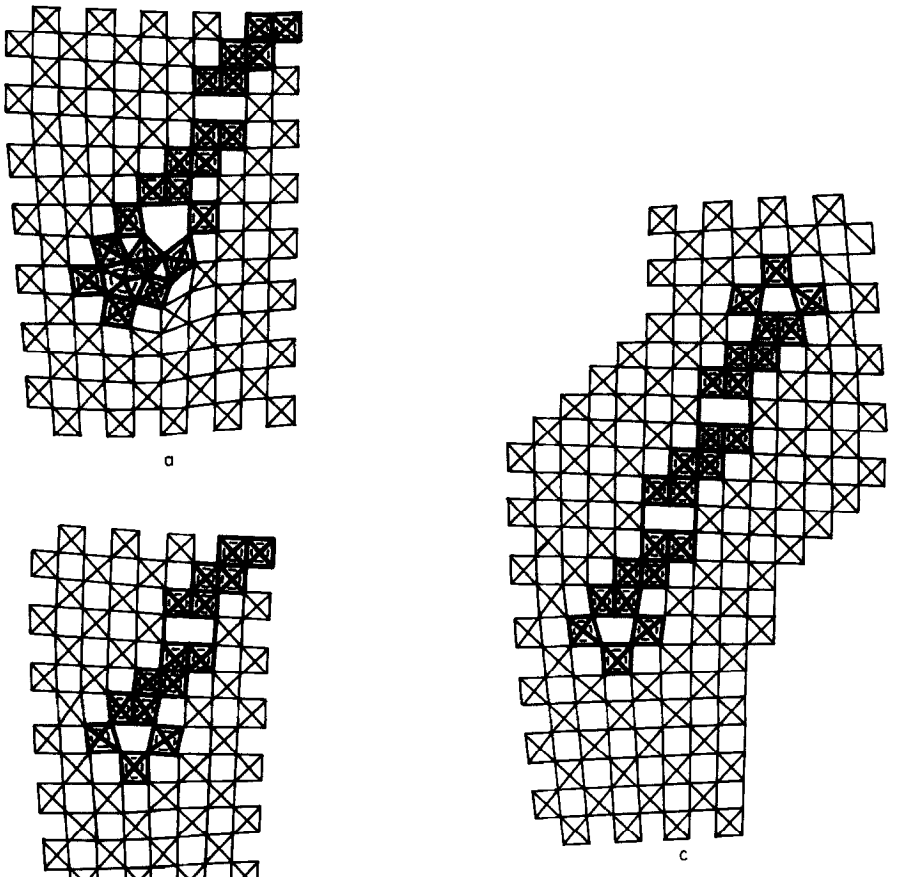

FIG. 12. Termination of (103) *CSP* by filled and empty pentagonal tunnels (a) or by a single empty pentagonal tunnel (b). (c) shows a very short (103) *CSP* terminated at both ends by empty pentagonal tunnels.

defects aggregate to form single *CSP* may be derived by consideration of Fig. 13. Here the smallest units of (104), or (001), and (103) and (102) *CSP* are shown (Figs. 13d,c, and b, respectively) terminated by pentagonal columns. An even smaller unit is given in Fig. 13a. Note that this simply corresponds to replacement of one $[WO_6]$ octahedron by two (a split-interstitial-octahedral pair!). Furthermore this defect is simply related to the (001) *CSP*-P defect as shown in Fig. 14a. (Corresponding defects are derived for (103) and (102) *CSP*-P in Figs. 14b,c.) Thus it is suggested that at relatively low or intermediate temperatures (say 300–700°C) single *CSP* precipitate by aggregation of *CSP*-P defects, with the topological transformations indicated in Fig. 14 occurring as the relatively coherent and mobile *CSP*-P defects become unstable under the influence of the octahedral tilts included in the tetragonal/orthorhombic/monoclinic transitions of the WO_{3-x} matrix (cf. Fig. 5). The transformation given in Fig. 14b may occur also as an intermediate stage in the precipitation of TTB columns (Fig. 15). Similarly the transformation of Fig. 14a may occur as an intermediate stage during the precipitation of PC–HT units (Fig. 11b). Here coalescence of two *CSP*-P

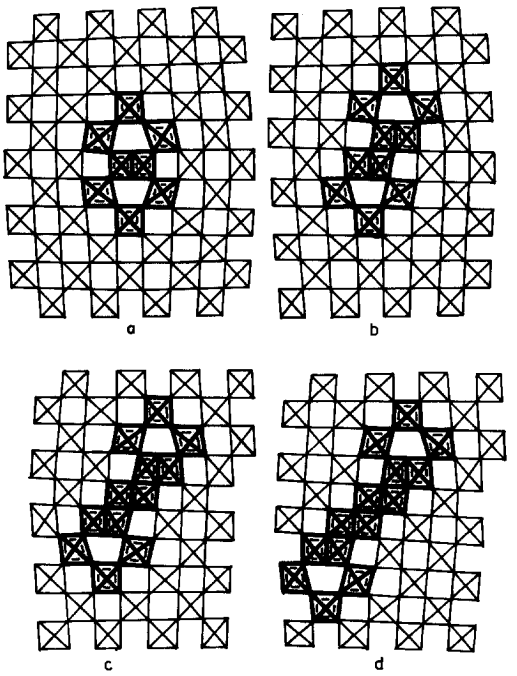

FIG. 13. Split-interstitial-octahedral-pair enveloped by WO_3 (a) (cf. Fig. 14a). (b), (c), and (d) show evolution of short (102), (103), and (104) *CSP* by addition of edge-shared pairs of octahedra.

units first gives rise to two empty pentagonal tunnels with a large irregularly shaped hole in between (Fig. 16b). Addition of two further *CSP*-P units (cf. Fig. 8) then fills the pentagonal columns at the same time as slight regroupings of octahedral linkages produce almost regular pentagonal and hexagonal tunnels (Fig. 16c). Thus *CSP*-P defects readily adapt to allow precipitation of both single *CSP* and their termination by simple pentagonal columns (Fig. 12c) or larger PC–HT arrays (Fig. 11b; see also Fig. 3b in Ref. (*10*)). Figure 6 of Ref. (*10*) shows a beautiful example of a mixed (103) *CSP*/PC–HT defect precipitated between neighboring *CSP*. Such observations are readily explained in terms of the above pictures whereby the structure of the precipitating extended defects is critically dependent on the precise temperature of precipitation, and hence will be very strongly dependent on the *rate* of cooling of the specimen. Specimens cooled relatively quickly should therefore show a mixture of extended defects in various states of aggregation.

(*e*) *Nucleation of New* CSP *Close to Existing* CSP

It has been reported (*23, 10, 7*) that new *CSP* are often observed to nucleate close to preexisting *CSP*, and it was even suggested that this indicated an oscillatory interaction potential associated with *CSP* (*23*). *CSP* precipitation will tend to occur when the WO_3 matrix has the tetragonal form, rather

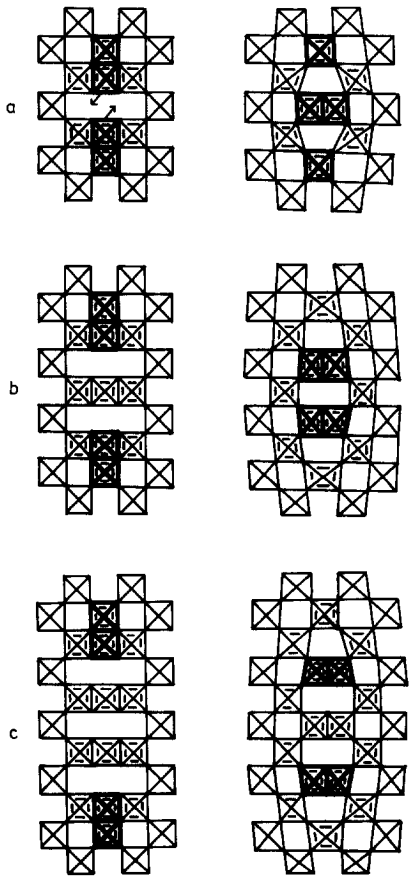

FIG. 14. Topological relationships between *CSP*-P defects with corresponding split-interstitial-octahedral structures, showing pentagonal tunnel terminations.

than the orthorhombic or tilted octahedral structure (section 2(a) above). It seems therefore that new *CSP* formed especially under relatively low temperature beam heating conditions, where the matrix is essentially monoclinic structure, will therefore prefer to form rather close to existing *CSP*, where the octahedral tilts are already relatively small. Direct evidence that the WO_3 matrix varies in structure between *CSP* has been obtained for a specimen of stoichiometry $(Nb,W)O_{2.933}$, containing (104) *CSP* of relatively large spacing (45–50 Å). For quite specific electron imaging conditions a $\sqrt{2}a \times \sqrt{2}a$ superstructure appeared in the region between *CSP*, gradually changing to $a \times a$ periodicity near the *CSP*. Further discussion of the electron optical study of this effect is left for a later publication (Bursill, in preparation).

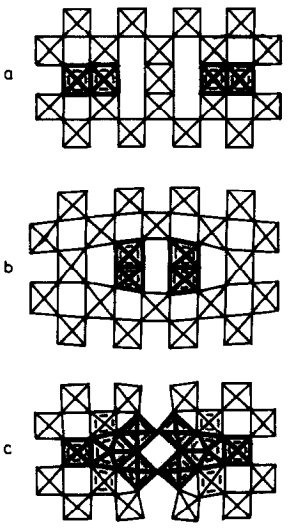

FIG. 15. Representation of transformation of two (103)-type *CSP*-P defects into a TTB defect. Transformation of a (103) *CSP*-P unit first gives rise to two empty pentagonal tunnels (b) which may then be filled by M^{5+} cations from a second *CSP*-P defect. Accompanying groupings of octahedral linkages gives rise to more regular pentagonal tunnels (cf. Fig. 9).

(*f*) *Comment on Beam-Heating Observations*

In situ observations in the electron microscope [*6, 7, 23*] often show a relatively diffuse band of contrast appearing between existing *CSP* or in the WO_3 matrix prior to growth of new *CSP*. The published images have insufficient resolution to allow the "interstitial" or "vacancy" nature of the precipitation mechanism to be established in these cases. The possibility that oxygen vacancy defects, suitably charge compensated by M^{5+} cations, may exist under some experimental conditions, cannot be discarded at this stage. Further HREM studies of the terminations of single *CSP* are required before it can be claimed that *CSP* growth *always* occurs by an "interstitial loop" mechanism.

Note also that the *CSP* precipitation mechanism may be surface initiated in thin foils, during observation in the electron microscope, and hence may involve quite different atomic mechanisms to precipitation within bulk WO_{3-x}. Experience with MoO_{3-x} [*30, 31*] suggests that complications may occur during *in situ* studies due to reaction of the specimen with absorbed OH^- ions.

In principle there will also be a finite "small defect" concentration, e.g., existing in equilibrium with extended defects. It may happen that at beam temperatures lower than the effective specimen preparation "quench" temperature (i.e., where kinetics prevented equilibrium being attained upon cooling) there will be further precipitation of small defects in an attempt to reach equilibrium at the lower temperature. The general question of the equilibrium concentration of small defects coexisting with extended defects must now become the subject of further controlled experimental study.

3. Conclusion

It should be significant that to date *in situ*

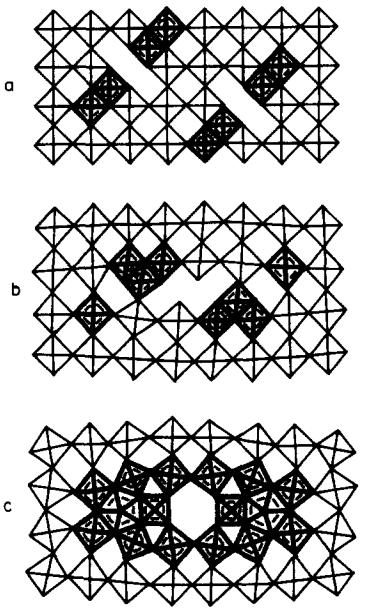

FIG. 16. Coalescence of two (001) *CSP*-P units (a) first gives rise to two empty pentagonal tunnels with a large irregularly shaped hole (b). Addition of two further *CSP*-P units (cf. Fig. 8b) then fills the pentagonal columns. Accompanying regroupings of octahedral linkages then give rise to regular pentagonal and hexagonal tunnels (c).

observations of the precipitation of *CSP* by beam heating in an electron microscope (*6, 7, 23*) have all involved relatively low temperatures. Often *CSP* appear under normal observation. Similarly most preparations of WO_{3-x} and doped WO_3 crystals have concerned specimens given well-controlled high temperature treatments (usually at temperatures much greater than 710°C) followed by *uncontrolled* cooling histories. Following our experience with TiO_{2-x} (*13–18*) we expect that *CSP* will be observed to precipitate predominantly as pairs, involving no incoherent terminating defects, in specimens cooled relatively very slowly across the phase boundary of tetragonal WO_{3-x}. Specimens cooled at intermediate rates should show a mixture of pairs and single *CSP* with PC–HT terminations and specimens quenched rapidly to ~300–700°C and then cooled relatively slowly should show predominantly PC–HT type precipitation. (*In situ* studies of doped specimens (Bursill, in preparation) have already confirmed some of the above predictions of the present structural considerations.) Clearly many interesting controlled experiments need to be performed to establish the details of the precipitation phenomena occuring *outside* the phase WO_{3-x}.

The nature of the structural defects responsible for nonstoichiometry *within* the phase WO_{3-x} seems to be reasonably well explained in terms of the *CSP*-pair small defect model introduced above. In another paper (Baumard, Blanchin, and Bursill, in preparation) the interpretation of physical property measurements of WO_{3-x} and TiO_{2-x} is discussed. It is shown that use of the new small defects models introduced above and in Ref. (*12*) provide an alternative, and more realistic, basis for the interpretation of the results of thermogravimetric electrochemical cell, electrical conductivity, internal friction, etc. experiments. Clearly the use of the principles of point defect equilibrium, with classical isolated interstitial, vacancy, or substitutional point defect models has now to be carefully reassessed.

Use of realistic small defect models, as recently introduced for TiO_{2-x} and WO_{3-x}, should enable the transport and optical properties of these important ceramic materials (see, e.g., Ref. (*3*)) to be more completely understood.

Image simulations of the contrast expected for the small *CSP*-pair-type defects show that it should be possible to directly image, and positively identify, such small defects, and their aggregates, using very specific HREM imaging conditions (Bursill, in preparation). The image given in Ref. (*23*), Fig. 8 is suggestive of the type of contrast expected. Further HREM observations are required.

Acknowledgments

This work was financially supported by the University of Melbourne. The author is indebted to Dr. M. G. Blanchin (Lyon, France) for stimulating discussions in the earliest stages of this work.

References

1. J. F. Marucco and A. Htiwech, *J. Solid State Chem.* **40,** 197–202 (1981).
2. C. Choain-Maurin and M. Fernand Marion, *C.R. Acad. Sci. Paris* **259,** 4700–4703 (1964).
3. J. M. Berak and M. J. Sienko, *J. Solid State Chem.* **2,** 109–133 (1970).
4. J. S. Anderson and B. G. Hyde, *J. Phys. Chem. Solids* **28,** 1393 (1967).
5. L. A. Bursill and B. G. Hyde, *J. Solid State Chem.* **4,** 430–446 (1972).
6. M. Sundberg and R. J. D. Tilley, *Phys. Status Solidi A* **22,** 677 (1974).
7. J. Booth, T. Ekström, E. Iguchi, and R. J. D. Tilley, *J. Solid State Chem.* **41,** 293–307 (1982).
8. K. Hiraga and B. G. Hyde, reported at Australian Electron Microscope Conference, Canberra, 1982.
9. S. Iijima and J. G. Allpress, *Acta Crystallogr. Sect. A* **30,** 29 (1974).
10. W. Sahle and M. Sundberg, *Chem. Scr.* **16,** 163–168 (1980).
11. L. Kihlborg, M. Sundberg, and A. Hussain, *Chem. Scr.* **15,** 182–186 (1980).
12. L. A. Bursill and M. G. Blanchin, *J. Phys.* Lett. **44,** L-165 (1983).
13. M. G. Blanchin, L. A. Bursill, J. L. Hutchison, and P. L. Gai, *J. Phys. Colloq.* **42,** C3–95 (1981).
14. L. A. Bursill, M. G. Blanchin, and D. J. Smith, *Proc. R. Soc. London Ser. A* **384,** 135 (1982).
15. D. J. Smith, M. G. Blanchin, and L. A. Bursill, *Micron.* **13,** 245 (1982).
16. L. A. Bursill, M. G. Blanchin, D. J. Smith, and A. Mebarek, "Point, Line, and Extended Defect Structures in Nonstoichiometric Rutile," from Proceedings, Fourth Europhysical Topical Conference on Lattice Defects in Ionic Crystals, Dublin, 1982; to be published in *Radiat. Eff.* (1983).
17. M. G. Blanchin, L. A. Bursill, and D. J. Smith, *Proc. R. Soc. London,* submitted (1983).
18. L. A. Bursill, D. J. Netherway, M. G. Blanchin, and D. J. Smith, *Proc. R. Soc. London,* submitted (1983).
19. M. Sundberg, *J. Solid State Chem.* **35,** 120–127 (1980).
20. T. Ekström and R. J. D. Tilley, *Chem. Scr.* **16,** 1–23 (1980).
21. M. Kawaminami and T. Hirose, *J. Phys. Soc. Japan* **46,** 864 (1979).
22. E. Salje, *Acta Crystallogr. Sect B* **33,** 574 (1977).
23. S. Iijima, *J. Solid State Chem.* **14,** 52 (1975).
24. S. Iijima and J. G. Allpress, *J. Solid State Chem. A* **30,** 29 (1974).
25. L. A. Bursill and B. G. Hyde, *Nature London* **240,** 122.
26. B. G. Hyde and M. O'Keefe, *Acta Crystallogr. Sect. A* **29,** 243 (1973).
27. P. Gado, *Acta Phys. Acad. Sci. Hung.* **18,** 111 (1965).
28. S. Andersson and A. D. Wadsley, *Nature London* **211,** 581 (1966).
29. J. van Landuyt and S. Amelinckx, *J. Solid State Chem.* **6,** 222 (1973).
30. L. A. Bursill, *Proc. R. Soc. London Ser. A* **311,** 267 (1969).
31. L. A. Bursill, W. C. T. Dowell, P. Goodman, and N. Tate, *Acta Crystallogr. Sect. A* **34,** 296 (1978).